INSTITUTE OF PHYSICS PUBLISHING JOURNAL OF PHYSICS A: MATHEMATICAL AND GENERAL

J. Phys. A: Math. Gen. **37** (2004) 8991–9021 PII: S0305-4470(04)80169-0

The contour deformation method in momentum space, applied to subatomic physics

G Hagen[1], **J S Vaagen**[1] **and M Hjorth-Jensen**[2]

[1] Department of Physics and Technology, University of Bergen, N-5000 Bergen, Norway
[2] Department of Physics and Center of Mathematics for Applications, University of Oslo, N-0316 Oslo, Norway

E-mail: gaute.hagen@ift.uib.no, jans.vaagen@ift.uib.no and morten.hjorth-jensen@fys.uio.no

Received 5 May 2004
Published 8 September 2004
Online at stacks.iop.org/JPhysA/37/8991
doi:10.1088/0305-4470/37/38/006

Abstract

A generalized contour deformation method (CDM), which combines complex rotation and translation in momentum space, is discussed. CDM gives accurate calculation of two-body spectral structures: bound, antibound, resonant and continuum states forming a Berggren basis. It provides a basis for full off-shell t-matrix calculations both for real and complex input energies. Results for both spectral structures and scattering amplitudes compare perfectly well with exact values for the analytically solvable separable non-local Yamaguchi potential as a testcase. Accurate calculation of antibound states in the Malfliet–Tjon and the realistic CD–Bonn nucleon–nucleon potential are presented. Calculation of antibound states in the CD–Bonn potential are not known to have been given elsewhere.

PACS numbers: 03.65.Nk, 24.30.Gd

(Some figures in this article are in colour only in the electronic version.)

1. Introduction

In nuclear physics, as in atomic physics, the expansion of many-body wavefunctions on single-particle bases, generated by a suitable potential has been a common practice. For a given potential the single-particle eigenstates form a complete set of states,

$$\mathbf{1} = \sum_b |\psi_{nl}\rangle\langle\psi_{nl}| + \frac{1}{2}\int_{-\infty}^{\infty} \mathrm{d}k\, k^2 |\psi_l(k)\rangle\langle\psi_l(k)|. \tag{1.1}$$

A proof of this completeness relation, more precisely known as the *resolution of unity*, is given by Newton [1]. The relation also applies to the binary interaction of say two nucleons and their relative motion. The sum is over the bound states in the system, while the integral is over the positive energy continuum states. The infinite space spanned by this basis is given by all square integrable functions on the real energy axis, known as the L^2 space, which forms

a Hilbert space. In the case of a confining harmonic oscillator potential there is an infinite number of bound states and no continuum integral.

During the last decade the exploration of nuclear driplines has pushed traditional single-particle methods to their limits of applicability. The traditional shell-model with harmonic oscillator single-particle wavefunctions works well in the regime of well-bound nuclei. Moving towards the driplines, however, the nuclei cease to be well bound, and coupling to continuum structures plays an important role. A modification of the shell model where bound, resonant and continuum states are treated on equal footing has been under development the last few years, and has become known as the *Gamow shell model*; see [2–6]. The first attempt to also include antibound states in a realistic nuclear calculation is that of Vertse *et al* [7], where the role of antibound states in the pole RPA description of the giant monopole resonance was investigated. Recently, the role of anti-bound states in the Gamow shell model description of halo nuclei has been discussed [8].

The study of two-body resonant structures has a long history in theoretical physics. There exists a variety of methods described in textbooks; see e.g. [1, 9–11]. Among the more popular methods are those of analytic continuation; the complex scaling method (CSM) and the method based on analytic continuation in the coupling constant (ACCC).

In this work, we consider an approach formulated for integral equations in momentum space. The method is based on deforming contour integrals in momentum space, and is known as the contour deformation or distortion method (CDM). It has been shown in [12] that a *contour rotation* in momentum space is equivalent to a rotation of the corresponding differential equation in coordinate space. The coordinate space analogue is often referred to as the *dilation group transformation* or *complex scaling*. The *dilation group transformation* was first formulated and discussed in [13, 14], and was developed to examine the spectrum of the Green's function on the second energy sheet.

The CDM formulated *in momentum space* is not new in nuclear physics. It was studied and applied in the 1960s and 1970s; see, for example, [15–18], especially in the field of three-body systems. Most of these references applied a *contour rotation* in momentum space. By restricting oneself to a rotated contour certain limitations and restrictions however appear in the equations, determined by the analytical structure of the integral kernels and potentials. In [18] a more sophisticated choice of contour, based on rotation and translation, was applied to the three-nucleon momentum space Faddeev equation for a separable Yamaguchi interaction. This choice of contour made it possible to avoid the logarithmic singularities of the Faddeev kernel and, hence, allowed for a continuation in energy to the non-physical energy sheet.

A revitalizing of the contour deformation method in momentum space is in place, given the new theoretical challenges of dripline physics. CDM is a method which allows for accurate and stable solutions of bound, anti-bound, capture and decay states. We consider a generalized type of contour, allowing for an analytic continuation into the third quadrant of the complex k-plane. Antibound and capture states near the scattering threshold may then be calculated at a specified accuracy. This choice of contour may be regarded as belonging to the *Berggren class* of contours [19]. Berggren [19], and later Lind [20], studied various completeness relations derived by analytic continuation of the completeness relation, stated in equation (1.1), to the complex plane. The Berggren completeness includes discrete summation over resonant as well as bound states. Our choice of contour differs from recent applications of the Berggren formalism (see e.g. [2–6]), in that the contour approaches infinity along complex rays in the complex k-plane as opposed to contours which approach infinity along the real k-axis. We will point out the intimate relationships between complex coordinate scaling, the general Berggren basis and the method of continuation of the scattering equations to the second energy sheet by contour deformation.

Complex scaling *in coordinate space* has for a long time been used extensively in atomic and molecular physics (see [21]). During the last decade it has also been applied in nuclear physics, as interest in loosely bound nuclear halo systems has grown (see e.g. [22–24]). Complex scaling in coordinate space is usually based on a variational method [21], and an optimal variational basis and scaling parameters have to be sought. One of the disadvantages of the coordinate space approach is that the boundary conditions have to be built into the equations, and convergence may be slow if the basis does not mirror the physical outgoing boundary conditions well.

There are several advantages in considering the contour deformation method in momentum space. First, most realistic potentials derived from field theoretical considerations are given explicitly in momentum space. Secondly, the boundary conditions are automatically built into the integral equations. Moreover, the Gamow states (physical resonances) [9] in momentum space are non-oscillating and rapidly decreasing, even for Gamow states with large widths, far from the real energy axis, as opposed to the complex-scaled coordinate space counterpart. The latter states are represented by strongly oscillating and exponentially decaying functions. Finally, numerical procedures are often easier to implement and check. Convergence is easily obtained by just increasing the number of integration points in the numerical integration.

If one restricts the deformation to a rotation of the contour, as studied in [15–17, 25, 26], one is not able to expose antibound states in the energy spectrum, since the maximum allowed rotation angle does not allow rotation into the third quadrant of the complex momentum plane. This limitation is sometimes used as an argument for advocating other approaches, such as the ACCC method; see the recent work of Aoyama [27]. We will show that by distorting the contour by *rotation and translation* into the third quadrant of the complex k-plane, we are able to introduce a new feature to the complex scaling method, namely *accurate calculation of antibound states as well as bound and resonant states*. CDM represents also an alternative to the so-called *exterior complex scaling* method. The *exterior complex scaling* method was just formulated to avoid intrinsic non-analyticities of the potential, and in this way calculation of resonances in *non-dilation* analytic potentials are made possible (see [21] and references therein).

The contour deformation method has also been applied to the solution of the full off-shell scattering amplitude (t-matrix); see [12, 16, 17, 28]. By rotating the integration contour, an integral equation is obtained with a compact integral kernel. This has numerical advantages as the kernel is no longer singular. As discussed in [16], a rotation of the contour gives certain restrictions on the rotation angle and maximum incoming/outgoing momentum in the scattering amplitude. We will again show that our extended choice of contour in momentum space avoids all these limitations and that an accurate calculation of the scattering amplitude can be obtained. Thus, the method we advocate allows us to give an accurate calculation of the full energy spectrum. Moreover, it yields a powerful method for calculating the full off-shell complex scattering amplitude (t-matrix). It is also rather straightforward to extend this scheme to in-medium scattering in, for example, infinite nuclear matter.

In section 2, we outline the CDM in momentum space and discuss its relation to the Berggren completeness, deriving the states of the Malfliet–Tjon nucleon–nucleon interaction as an example. The corresponding Berggren basis is used for convergence studies. As an additional example the states of the CD–Bonn interaction [29] are also calculated, the antibound state for the first time. In section 3, the Berggren representation of the full off-shell t-matrix is given, together with various applications of CDM to the scattering of the Malfliet–Tjon interaction [30]. Section 4 gives expansion of the eigenvalue problem for the analytically solvable separable non-local Yamaguchi [10, 31] interaction on a Malfliet–Tjon Berggren basis. Comparison between analytic and numerical results are given for antibound

and resonant states. Finally, in section 5, we study the expansion of a resonant state generated by a Gaussian interaction on a Berggren basis given by the Malfliet–Tjon interaction. The energy and wavefunction are studied as a function of cutoff in momentum/energy of the complex continuum states entering the Berggren completeness.

2. Berggren spectral decomposition in momentum space

2.1. The contour deformation method

The momentum space Schrödinger equation, for relative motion in partial wave l in a central potential, reads

$$\frac{\hbar^2}{2\mu}k^2\psi_{nl}(k) + \frac{2}{\pi}\int_0^\infty \mathrm{d}q\, q^2 V_l(k,q)\psi_{nl}(q) = E_{nl}\psi_{nl}(k). \tag{2.1}$$

With real momenta the momentum space Schrödinger equation corresponds to a hermitian Hamiltonian. The energy eigenvalues will in this case always be real, corresponding to discrete bound states ($E_{nl} < 0$) and a continuum of scattering states ($E_{nl} > 0$). Resonant and antibound states can never be obtained by directly solving equation (2.1), as it stands. In a sense, one can say that the spectrum of a hermitian Hamiltonian does not display all information about the physical system.

Generalizing k to the complex k-plane, i.e. $k = \mathrm{Re}[k] + \mathrm{iIm}[k]$, an integral equation for the bound state wavefunctions appearing in equation (2.1) may be written as

$$\psi_{nl}(k) = \frac{1}{E_{nl} - k^2/2\mu}\frac{2}{\pi}\int_0^\infty \mathrm{d}q\, q^2 V_l(k,q)\psi_{nl}(q). \tag{2.2}$$

$\psi(k)$ is analytic in the upper-half complex k-plane corresponding to the physical energy sheet, except for simple poles at the bound state energies (positive imaginary k) and a cut in the complex E-plane along the real energy axis. The interaction between the particles, $V_l(k, q)$ is assumed to be spherically symmetric without tensor components. Our discussion does not involve the particle spins explicitly. The Fourier–Bessel transform of a non-local potential $V_l(r, r')$ in coordinate space is given by

$$V_l(k,k') = \int_0^\infty \mathrm{d}r\, r^2 \int_0^\infty \mathrm{d}r'\, r'^2\, j_l(kr)\, j_l(k'r')V_l(r,r'). \tag{2.3}$$

In the case of a local potential,

$$V_l(r,r') = \frac{\delta(r-r')}{r^2}V_l(r),$$

and equation (2.3) reduces to

$$V_l(k,k') = \int_0^\infty \mathrm{d}r\, r^2\, j_l(kr)\, j_l(k'r)V_l(r). \tag{2.4}$$

The interaction in momentum space is given in units of MeV fm^3.

In the following we study and explore the resonant and antibound state spectra by the contour deformation method.

Antibound states are not to be interpreted as physical states, i.e. a quantal system cannot be put in such a state. Nevertheless, antibound states close to the scattering threshold may have impact on observables such as phase shifts. For a system with antibound states close to the scattering threshold, a large enhancement of the scattering cross-section will take place. This enhancement can be understood in terms of the antibound states; see [8] for a discussion of scattering wavefunctions close to threshold in the presence of a nearby bound or antibound

state. From a mathematical point of view an antibound state is defined as a pole of the scattering matrix located on the negative imaginary k-axis.

Resonant states can be divided into two subclasses: decay and capture states. Decay states are associated with poles of the scattering matrix located in the fourth quadrant of the complex k-plane. They have outgoing boundary conditions at infinity. Capture states are on the other hand associated with poles in the third quadrant of the complex k-plane, and have incoming waves at infinity. Naturally only capture states can be given physical meaning. Capture states may be interpreted as quasi-stationary states formed inside a potential barrier in the positive energy regime.

Resonant states will have a definite lifetime before they decay through the barrier. This lifetime varies inversely with the probability of tunnelling through the barrier, and the probability of tunnelling is given by the width Γ of the resonant states. The width is in turn given by the absolute value of the imaginary part of the resonance energy squared. The closer the resonance energy is to the real energy axis, the smaller the width becomes and the lifetime of the quasi-stationary states increases. This indicates that resonant states with energy close to the real energy axis may have larger impact on observable quantities, e.g. phase shifts and scattering cross-sections. Physical decay states are those with positive real energy. Gamow states are to be understood as physical resonant decay states close to the real energy axis, i.e. resonant states with narrow widths. In [9] a more detailed discussion of the interpretation and physical understanding of resonant states is given.

Antibound and resonant states are located on the second (non-physical) energy Riemann sheet. The momentum is a multivalued function of energy; $k(E) = \sqrt{2\mu E}$. Multivalued functions may be represented by Riemann surfaces of branch cuts. The upper-half complex k-plane and the lower-half complex k-plane maps into the same complex energy plane. This problem is resolved by defining a Riemann surface with two sheets. The physical energy sheet (first sheet) is a mapping of the upper-half complex k-plane while the so-called *non-physical* energy sheet (second sheet) is a mapping of the lower-half complex k-plane (see e.g. [1]). To reach into the non-physical energy sheet where antibound and resonant states are to be found one has to analytically continue the scattering equations through the cut along the real energy axis and into the lower-half complex energy plane. We study here the analytic continuation of equation (2.1) into the non-physical sheet by the contour deformation method. Such a transformation of equation (2.1) can be obtained by an analytic continuation of the completeness relation of equation (1.1) to the complex k-plane.

Resonances are not normalizable in the normal sense. Due to their exponentially growing and oscillatory behaviour along the real r-axis the norm integral is divergent. Nevertheless, divergent integrals may be given a definite value by some regularization procedure. Zel'dovich [11] was the first to propose such a regulariztion procedure for making the norm integrals of resonances definite by adding a convergence factor $\exp(-\epsilon r^2)$ and then taking the limit $\epsilon \to 0$. This procedure is most convenient in analytic cases; in numerical applications taking the limit $\epsilon \to 0$ is difficult. Another regularization procedure which is more tractable from a numerical standpoint, is the method proposed by Gyarmati and Vertse [32]; they regularized the norm integrals by a complex rotation in the radial coordinate after a finite radial distance R. This procedure introduces an exponential damping to the growing oscillatory behaviour of the resonant wavefunctions, and numerical implementation of expectation values involving resonant states is made possible.

In the 1960s, Berggren discussed the use of resonant states in eigenfunction expansions of scattering and reaction amplitudes; see [19, 33–35]. He used the regularization procedure by Zel'dovich for resonant states. The resonant states form an incomplete set of states, and for completeness the non-resonant continuum states has to be taken into account. Berggren found

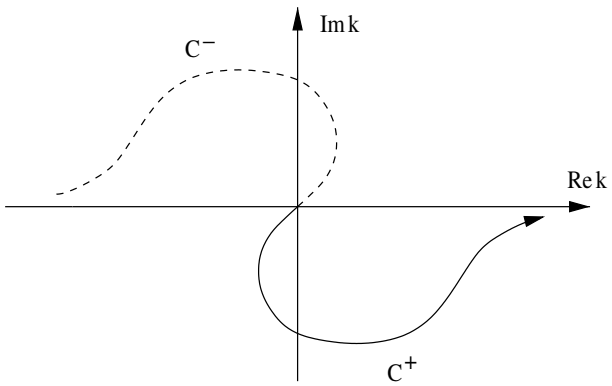

Figure 1. Plot of a general inversion symmetric contour $C = C^+ + C^-$ in the complex k-plane: C^+ is given by the solid line, while C^- is given by the broken line.

that the regularized resonant states along with a set of non-resonant continuum states defined on deformed contours in the complex momentum plane, form a bi-orthogonal set of states. This bi-orthogonal set can in turn be used as expansion basis for various physical quantities, where the resonant character of the system is displayed explicitly.

The method Berggren studied is based on analytic continuation of the completeness relation (see equation (1.1)) to the complex k-plane by deforming the integration contour. We give here a brief summary of the procedure which considers the integral in equation (1.1) as an integral over the contour $\Gamma = S + C$, where the contour C is defined on the real k-axis from $-\infty$ to $+\infty$ and the contour S is given by an infinite semicircle in the upper-half complex k-plane closing the contour Γ. The sum over bound states are then the residues calculated at the poles of the scattering matrix along the positive imaginary k-axis. The integration along the real axis may then be distorted into some *inversion symmetric* contour, meaning that if k is on C, then $-k$ is also on C. By redefining the completeness relation on distorted contours in the complex k plane, one can show by using Cauchy's residue theorem that the summation over discrete states will in general include bound, antibound and resonant states [20, 33]. By this procedure the norm integral of the resonant states is regularized along the distorted contours. In [20] completeness relations for various *inversion symmetric* contours in the complex k-plane were derived and discussed; all inversion symmetric contours will hereafter be labelled *Berggren class* of contours. The eigenfunctions defined along distorted contours form a *biorthogonal* set, and the normalization follows the generalized c-product [20, 21]

$$\langle\langle\psi_{nl}|\psi_{n'l}\rangle\rangle \equiv \langle\psi^*_{nl}|\psi_{n'l}\rangle = \delta_{n,n'}. \tag{2.5}$$

The most general completeness relation on an arbitrary *inversion symmetric* contour (see figure 1) $C = C^+ + C^-$ can then be written as

$$\mathbf{1} = \sum_{n\in\mathbf{C}} |\psi_{nl}\rangle\langle\psi^*_{nl}| + \int_{C^+} \mathrm{d}k\, k^2 |\psi_l(k)\rangle\langle\psi^*_l(k)|, \tag{2.6}$$

where C^+ is the distortion of the positive real k-axis, and C^- the distortion of the negative real k-axis.

Here the symmetry of the integrand has been taken into account, that is

$$\int_{C^-} \mathrm{d}k\, k^2 |\psi_l(k)\rangle\langle\psi^*_l(k)| = \int_{C^+} \mathrm{d}k\, k^2 |\psi_l(k)\rangle\langle\psi^*_l(k)|.$$

The summation is over all discrete states (bound, antibound and resonant states) located in the domain $\mathbf{C}$, defined as the area above the contour C, and the integral is over the non-resonant

complex continuum defined on C^+. The space spanned by the basis given in equation (2.6) includes all square-integrable functions defined in the domain $\mathbf{C}$, defining a generalized Hilbert space. The complete basis could then be used to expand other resonant and antibound states (belonging to another Hamiltonian), defined in the region above the distorted contour. Such a complete basis is more flexible than a complete basis defined for only real energies. From the general completeness relation (2.6) one can deduce the corresponding eigenvalue problem, $H|\psi\rangle = E|\psi\rangle$. This eigenvalue problem represents the analytically continued Schrödinger equation onto a general distorted contour C^+ in the complex k-plane. The Hamiltonian will in this case be complex and non-hermitian, as Gamow and antibound states are included in the spectrum.

Above we discussed how a complex and non-hermitian eigenvalue value problem may be obtained by analytic continuation of the completeness relation through the cut and into the second (non-physical) energy sheet. In close analogy with the above discussion on completeness relations, the momentum space Schrödinger equation (2.1), defined on the positive real k-axis, may be directly continued to the lower-half complex k-plane. Thereafter a general completeness relation, like equation (2.6), may be inferred. We must emphasize that the requirement that the distorted contour must be *inversion-symmetric* is not sufficient when continuing the Schrödinger equation (2.1) into the third quadrant of the complex k-plane.

In analytic continuation of integral equations we state the general rule (see e.g. [9]):

Continuing an integral in the complex plane, the moving singularities of the integrand must not intercept the integration contour.

Applying the contour deformation method to the momentum space Schrödinger equation (2.1), we must deform the contour in such a way that an intercept with the singularities is avoided. The only moving singularities of the integral kernel in equation (2.1) are contained in the potential. The analytic continuation of equation (2.1) to the lower-half complex energy plane is a stepwise process where overlapping domains of analyticity are created. Each step of analytic continuation of the Schrödinger equation to the complex energy plane involves the following three steps:

(i) The analyticity domain, D_1, for the wavefunction $\psi(k)$ is determined (see equation (2.2)). Except at the spectrum of the Hamiltonian, the analyticity of $\psi(k)$ is given by the potential $V(k, q)$, where q is real in the first step.

(ii) Having determined the analyticity region D_1 in the lower-half k-plane, the integration in q along the real axis may be distorted onto a contour C_1^+ in the lower-half complex k-plane. All points on the contour C_1^+ must be contained in the analyticity domain D_1.

(iii) A new analyticity domain D_2 is determined for the wavefunction $\psi(k)$. The domain D_2 is again determined by the singularity structure of the potential $V(k, q)$ where q is now on the distorted contour C_1^+. If and only if the contour C_1^+ also lies in the new domain of analyticity D_2, we may choose k on C_1^+ as well. This gives a closed integral equation, and the Schrödinger equation is transformed onto the contour C_1^+.

This process of analytic continuation may be continued iteratively uncovering larger domains of interest in the complex energy plane. The choice of contour must therefore be based on the following.

- The contour must be *inversion-symmetric*.
- The contour must be located in overlapping domains of analyticity (see step (iii) above) and the wavefunction must admit analytic continuation onto the contour C^+.
- The choice of contour must be based on an *a posteriori* knowledge of poles in each partial wave of the scattering matrix.

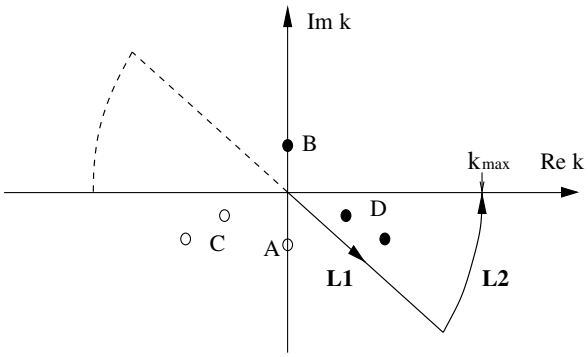

Figure 2. Contour $C_R^+ = L_1 + L_2$ is given by the solid line, while the contour C_R^- is given by the broken line. The contour $C_R = C_R^+ + C_R^-$ is clearly *inversion-symmetric*. The two-body spectrum which is exposed by this contour is marked by filled circles and the excluded spectrum by open circles. The full spectrum includes bound states (B), antibound (A), decay (D) and capture (C) resonant states.

The analytically continued equation (2.1) on a general inversion symmetric contour then takes the form

$$\frac{\hbar^2}{2\mu}k^2\psi_{nl}(k) + \frac{2}{\pi}\int_{C^+} \mathrm{d}q\, q^2 V_l(k,q)\psi_{nl}(q) = E_{nl}\psi_{nl}(k). \tag{2.7}$$

Here both k and q are defined on the inversion symmetric contour C^+ in the lower-half complex k-plane, giving a closed integral equation. The eigenfunctions satisfy the general completeness relation given in equation (2.6) and are normalized according to the general c-product.

In the following we study two distorted contours C_R^+ and C_{R+T}^+. These contours can be regarded as a special case of the *Berggren class* of contours. The contour C_R^+ is obtained by a phase transformation (rotation) into the lower-half complex k-plane while the second contour C_{R+T}^+ will be based on rotation followed by translation in the lower-half complex k-plane. These contours approach infinity along complex rays, and not *along* the real k-axis, although as $|k| \to \infty$ they should approach the real k-axis to define a closed integration contour. It has previously been assumed as a requirement for the choice of distorted contours that they approach infinity along the real k-axis (see e.g. [3]).

First we consider the contour C_R^+ given by two line segments L_1 and L_2. Line L_1 is given by $k = |k|\exp(-\mathrm{i}\theta)$ where $|k| \in [0, k_{\max}]$, L_2 by $k = k_{\max}\exp(-\mathrm{i}\theta)$; here $k_{\max}$ is a real and positive constant. One can easily show that for an exponentially bounded potential in coordinate space the integral in equation (2.1) along the arc L_2 will tend to zero for $k_{\max} \to \infty$. In this case the contour C_R^+ reduces to the line L_1. Figure 2 shows the contour C_R^+ along with the exposed and excluded two-body spectrum in the complex k-plane, which this choice of contour implies. The contour C_R^+ is part of the *inversion symmetric* contour $C_R = C_R^+ + C_R^-$, also indicated in figure 2.

Most potentials are of such analytic structure; that an analytic continuation into the fourth quadrant of the complex k-plane is possible, except on the imaginary k-axis. One may then uncover arbitrary large portions of the fourth quadrant of the second energy sheet, where resonances may be located. The analytically continued equation (2.7) onto the contour C_R^+ is obtained by the transformation $k = |k|\exp(-\mathrm{i}\theta)$ and $q = |q|\exp(-\mathrm{i}\theta)$. In this case, equation (2.7) is the momentum space version of the complex-scaled Schrödinger equation in coordinate space, discussed in e.g. [12]. A rotation in momentum space, $|k|\exp(-\mathrm{i}\theta)$, is equivalent to the

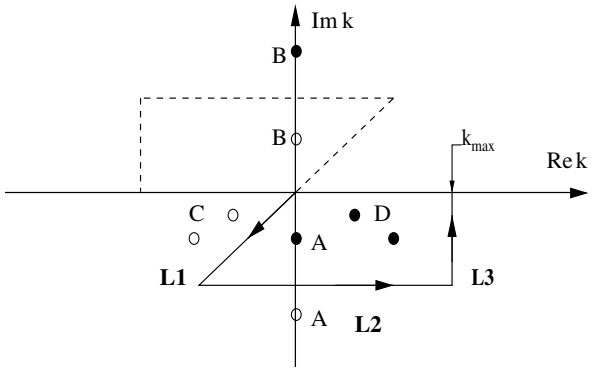

Figure 3. Contour $C^+_{R+T} = L_1 + L_2 + L_3$ is given by the solid line, while the contour C^-_{R+T} is given by the broken line. The contour $C_{R+T} = C^+_{R+T} + C^-_{R+T}$ is clearly *inversion-symmetric*. The two-body spectrum which is exposed by this contour is marked by filled circles (●) and the excluded spectrum by open circles (○). The full spectrum includes bound states (B), antibound (A), decay (D) and capture (C) resonant states.

complex scaling $r\exp(\mathrm{i}\theta)$ in coordinate space. The phase transformation $k \to |k|\exp(-\mathrm{i}\theta)$ turns out to be a similarity transformation (see e.g. [36]). The restriction on the rotation angle θ for the phase transformation may be shown to be $\theta < \pi/2$. This implies that antibound states cannot be included in the spectrum by this choice of contour.

Next we consider the contour obtained by rotation followed by translation in the lower-half complex k-plane. The contour C^+_{R+T} consists of three line segments. The line segment L_1 is given by a rotation $k = |k|\exp(-\mathrm{i}\theta)$ with $|k| \in [0, b]$, whereas L_2 is given by a translation $k = \mathrm{Re}[k] - b\sin(\theta)\mathrm{i}$ with $\mathrm{Re}[k] \in [b\cos(\theta), k_{\max}]$ and b determines the translation into the lower-half k-plane and, finally, L_3 is defined by $k = k_{\max} - \mathrm{Im}[k]\mathrm{i}$ with $\mathrm{Im}[k] \in [b\sin(\theta), 0]$. For $k_{\max} \to \infty$, the contribution to the integral in equation (2.1) along the line segment L_3 will vanish, and the contour C^+_{R+T} reduces to the line segments L_1 and L_2. Figure 3 shows the contour $C^+_{R+T} = L_1 + L_2 + L_3$ along with the exposed and excluded two-body spectrum which this choice of contour implies. The contour C^+_{R+T} is part of the *inversion symmetric* contour $C_{R+T} = C^+_{R+T} + C^-_{R+T}$ clearly seen in the figure.

Whether one chooses to solve the Schrödinger equation on the contour C^+_R or on the contour C^+_{R+T} depends on the problem under consideration. The singularity structure of a general potential is such that an analytic continuation onto a rotated contour in the third quadrant may not be achieved. However, by choosing a modified contour like C^+_{R+T} which avoids the non-analytic regions of the potential this may be possible. By solving the Schrödinger equation on the distorted contour C^+_{R+T} rotated into the third quadrant of the complex k-plane, we expose a part of the negative imaginary k-axis where antibound states may be located. In doing this we must emphasize that at the same time we are excluding a part of the positive imaginary k-axis where bound states may be located. This reminds us that the contour should be chosen relative to the partial wave component under study, i.e. a separate analysis has to be made for each partial wave.

2.2. Analyticity of the Malfliet–Tjon interaction in the complex momentum plane

As an illustration we consider the frequently used Malfliet–Tjon nucleon–nucleon (NN) interaction [30], which is a superposition of Yukawa terms. The interaction is in a coordinate

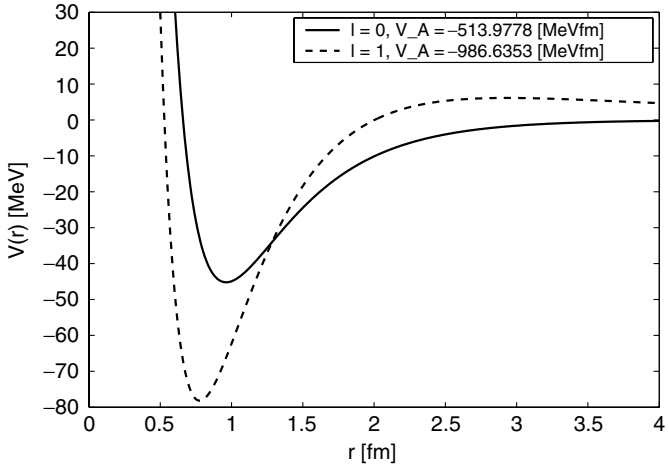

Figure 4. Plot of the $l = 0$ and the $l = 1$ Malfliet–Tjon interaction in coordinate space with angular momentum barrier included.

representation, given by

$$V(r) = V_R \frac{\exp(-\mu_R r)}{r} + V_A \frac{\exp(-\mu_A r)}{r}. \tag{2.8}$$

Here V_R and V_A are the repulsive and attractive strength of the interaction, respectively.

We employ conventional units, i.e. r (fm), k (fm^{-1}), $\mu_{R,A}$ (fm^{-1}) and $V_{R,A}$ (MeV fm). The interaction in coordinate space is given in units of MeV, while in momentum space in units of MeV fm^3. The reduced neutron–proton mass is $m_{np}c^2 = 938.926/2$ MeV.

It is known that the $^1S_0$ channel in the nucleon–nucleon interaction supports an antibound state near the scattering threshold. By choosing interaction parameters

$$V_R = 7.291 \times \hbar c \approx 1438.71\,\text{MeV fm}, \qquad \mu_R = 613.69/\hbar c \approx 3.11\,\text{fm}^{-1},$$

$$\mu_A = 305.86/\hbar c \approx 1.55\,\text{fm}^{-1}, \qquad V_A = -2.6047 \times \hbar c \approx -513.98\,\text{MeV fm},$$

the Malfliet–Tjon interaction resembles the form of a realistic nucleon–nucleon interaction with attractive and repulsive parts in the $^1S_0$ channel. It reproduces the $^1S_0$ phase shift in nucleon–nucleon scattering rather well, and supports an antibound state near the scattering threshold. In the following the parameters V_R, μ_R and μ_A are fixed to the values given above. We will however allow for a variation of the attractive strength V_A. This interaction will then still support bound and antibound states for s-waves, and for higher angular momentum resonances may also appear. Figure 4 gives a plot of the $l = 0$ and the $l = 1$ Malfliet–Tjon interaction in coordinate space with an angular momentum barrier included. For a given partial wave l, the Fourier–Bessel transform of equation (2.8) gives an analytic expression

$$V_l(k,k') = V_R \frac{1}{2kk'} Q_l(x_R) + V_A \frac{1}{2kk'} Q_l(x_A). \tag{2.9}$$

Here $Q_l(x)$ is the Legendre function of the second kind. The arguments of the Legendre function are $x_{R,A} = (k^2 + k'^2 + \mu_{R,A}^2)/2kk'$. Figure 5 gives a plot of the $l = 0$ Malfliet–Tjon interaction in momentum space for the interaction parameters given above.

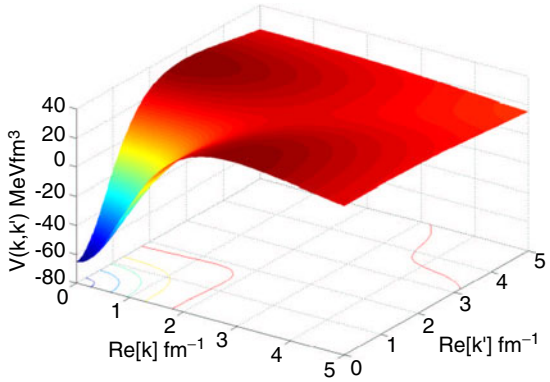

Figure 5. Plot of the $l = 0$ Malfliet–Tjon interaction in momentum space, for real k, k'.

We will give a demonstration of how the momentum space Schrödinger equation for the Malfliet–Tjon interaction may be continued to the non-physical energy sheet, i.e. the lower-half complex k-plane. The only moving singularities of the integral kernel in equation (2.7) are contained in the interaction itself; see equation (2.9). The singularity structure of the interaction is that of the Legendre functions. The Legendre functions are singular for $x = \pm 1$, and this determines the analyticity region of the interaction in the complex k-plane. Thus equation (2.9) is singular for

$$(k - k')^2 + \mu_{R,A}^2 = 0 \tag{2.10}$$

and

$$(k + k')^2 + \mu_{R,A}^2 = 0. \tag{2.11}$$

Equation (2.10) is satisfied for

$$\mathrm{Re}[k] = \mathrm{Re}[k'] \wedge \mathrm{Im}[k] = \pm\mu + \mathrm{Im}[k'],$$

and equation (2.11) for

$$\mathrm{Re}[k] = -\mathrm{Re}[k'] \wedge \mathrm{Im}[k] = \pm\mu_{R,A} - \mathrm{Im}[k'].$$

For k real and k' complex, we see from equation (2.11) that the interaction is singular for $\mathrm{Im}[k'] = \pm\mu_{R,A}$. In the first step of the continuation we keep k real and distort the path of integration into some contour C_1^+ in the analyticity domain $D_1 : -\mu < \mathrm{Im}[k] < \mu$, where we have defined $\mu = \min[\mu_R, \mu_A]$. This defines a new analyticity domain in the complex k-plane, determined by the analytic structure of $V_l(k, k')$, where k' is defined on the contour C_1^+, i.e. $D_2 : -\mu - C_1 < \mathrm{Im}[k] < \mu - C_1$. If the distorted contour C_1^+ lies in the overlapping domain $D_1 \cap D_2$, k may be defined on the contour C_1^+ as well, giving a closed integral equation. This procedure may be continued ad infinitum, uncovering the complete fourth quadrant of the complex k-plane. Solving the eigenvalue problem by the contour deformation method one may choose a purely rotated contour C_R^+, or a rotated + translated contour C_{R+T}^+, where $\theta < \pi/2$. Both contours will expose the resonant structures in the fourth quadrant of the complex k-plane.

For antibound states in the Malfliet–Tjon interaction, one must choose a contour of the type C_{R+T}^+ which consists of a rotation into the third quadrant and a finite translation in the lower-half complex k-plane. It can be easily shown that the translated part of the contour

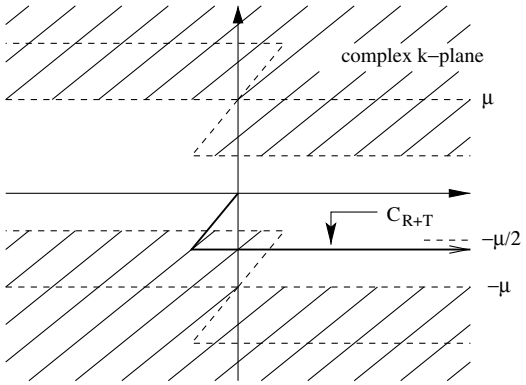

Figure 6. The white area gives the domain of overlapping analyticity for the momentum space Schrödinger equation for a rotated + translated contour, for a translation $|\mathrm{Im}[k]| > \mu/2$. The contour C^{+}_{R+T} is partly located outside the overlapping analyticity domain $D_1 \cap D_2$.

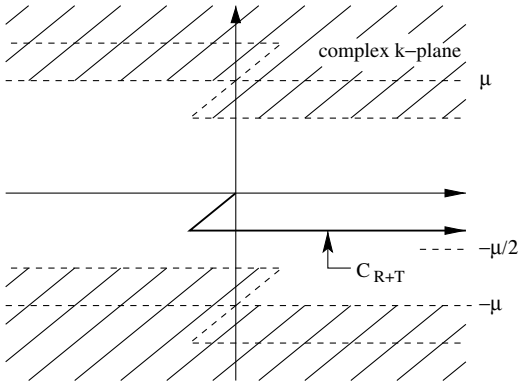

Figure 7. The white area gives the domain of overlapping analyticity for the momentum space Schrödinger equation for the C_{R+T} contour, with a translation $|\mathrm{Im}[k]| < \mu/2$. The contour is located inside the overlapping analyticity domain $D_1 \cap D_2$.

C^{+}_{R+T} has to be bounded by $|\mathrm{Im}[k]_{\max}| < \mu/2$. If the translation into the complex k-plane exceeds $\mu/2$, it is not possible to construct overlapping domains of analyticity which contain the distorted contour; see figure 6 for an illustration of this point. Figure 7 shows how the distorted contour C^{+}_{R+T} is contained in the overlapping analyticity domains, $D_1 \cap D_2$, for a translation $|\mathrm{Im}[k]| < \mu/2$.

By imposing a lower bound on the translated line segment C_T, given by $|\mathrm{Im}[k]| < \mu/2$, an exploration of antibound states is possible for the Malfliet–Tjon interaction. This limitation of the translation into the lower-half k-plane for the Malfliet–Tjon interaction is related to what is known as the Yukawa cut; in [1] it is shown that the Yukawa interaction has a cut along $\mathrm{Im}[k] \leqslant \mu/2$.

2.3. Antibound and resonant states of the Malfliet–Tjon interaction

Table 1 gives results of a calculation of the antibound neutron–proton s-wave ($l = 0$) state of the Malfliet–Tjon interaction, for increasing strength $V_A = \nu_A \times \hbar c$, where we have introduced the dimensionless quantity ν_A. With our choice of interaction parameters we have

Table 1. Calculation of the neutron–proton antibound state as function of increasing attractive strength ν_A for the s-wave Malfliet–Tjon interaction using the deformed integration path C^+_{R+T}. ν_A is dimensionless, and should be multiplied by $\hbar c$ to give the conventional units. The convergence is illustrated by increasing the number of integration points. Column A used $N1 = 30$, $N2 = 50$ integration points; column B used $N1 = 100$, $N2 = 100$ integration points and column C used $N1 = 150$, $N2 = 250$ integration points. Energy E is given in units of MeV.

	CDM			[37]
	A	B	C	D
ν_A	E	E	E	E
−2.6047	−0.066674	−0.066653	−0.066653	−0.06663
−2.5	−0.310114	−0.310115	−0.310115	−0.31004
−2.3	−1.229845	−1.229845	−1.229845	−1.22970
−2.1	−2.679069	−2.678979	−2.678979	−2.67878

$\mu = \min[\mu_R,\ \mu_A] = 1.55$ fm, which gives a maximum translation into the lower-half k-plane, $\mathrm{Im}[k]_{\max} = 1.55/2 \approx 0.775\ \mathrm{fm}^{-1}$. This means that all antibound states on the second energy sheet located in the energy domain $E \in [-24.9, 0]$ MeV may be included in the spectrum. For our calculation we use the rotation angle $\theta = 2\pi/3$ and a translation $|\mathrm{Im}[k]| = 0.5 \sin(2\pi/3) \approx 0.433\ \mathrm{fm}^{-1}$. This choice of contour will uncover the portion $E \in [-7.78, 0]$ of the negative energy axis on the second (non-physical) energy sheet. We see that all antibound states which may have an impact on phaseshifts may be included by this choice of contour. The convergence of the calculations is illustrated by increasing the number of integration points. As we obtained convergence of the antibound state energies by increasing the number of integration points, we are led to conclude that our results are stable; furthermore, comparison with the calculations of Elstel *et al* [37] shows only a small difference in the calculated values for the antibound state. In [37] the energy spectrum on the second energy sheet was calculated by analytic continuation of the t-matrix to the second energy sheet, and thereby searching for poles.

In calculating resonant states in the Malfliet–Tjon interaction, any deformed contour in the fourth quadrant of the complex k-plane will do, as long as the resonant states are enclosed by the contour and the real k-axis. The Malfliet–Tjon interaction supports resonant states for angular momentum $l \geqslant 1$, for which an angular momentum barrier is created and resonant states may be formed inside the barrier.

The $l = 1$ partial wave component of the Malfliet–Tjon interaction, supports bound, antibound and resonant states for a given ν_A. Figure 8 shows the trajectory of the imaginary part of the bound and antibound state pole in the complex k-plane as a function of interaction strength ν_A. The calculations were done on the contour C^+_{R+T}, rotated into the third quadrant of the complex k-plane. For decreasing interaction strength the bound and antibound states move toward the real axis. It can be seen that for a given interaction strength ν_A they are not located symmetrically with respect to the real k-axis, the antibound state being closer to the scattering threshold than the corresponding bound state. This is in agreement with the general rule that, for $l \geqslant 1$, the number of antibound states between the loosest bound state and the threshold is odd (see e.g. [1]). For $|\nu_A| \approx 5.47$, the bound and antibound states merge and are both annihilated. This occurs at zero energy ($\mathrm{Im}[k] = 0\ \mathrm{fm}^{-1}$), and is defined as the branching point. For $|\nu_A| < 5.47$ the bound and antibound states develop into decay and capture resonant states, respectively, moving symmetrically with respect to the imaginary k-axis in the lower-half k-plane.

Figure 9 shows how the bound state of the system approaches the scattering threshold and develop into decay resonant states for decreasing interaction strength ν_A. The interaction

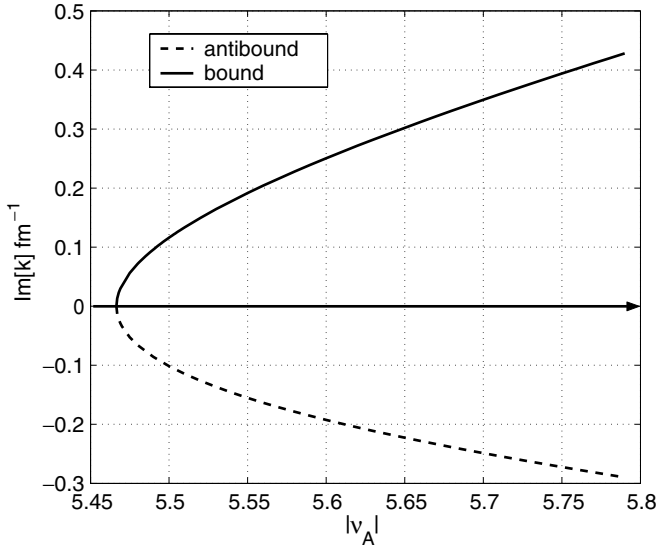

Figure 8. Plot of the bound and antibound state pole trajectory for the $l = 1$ component of Malfliet–Tjon interaction. The location of the poles along the imaginary k-axis is plotted as a function of interaction strength v_A.

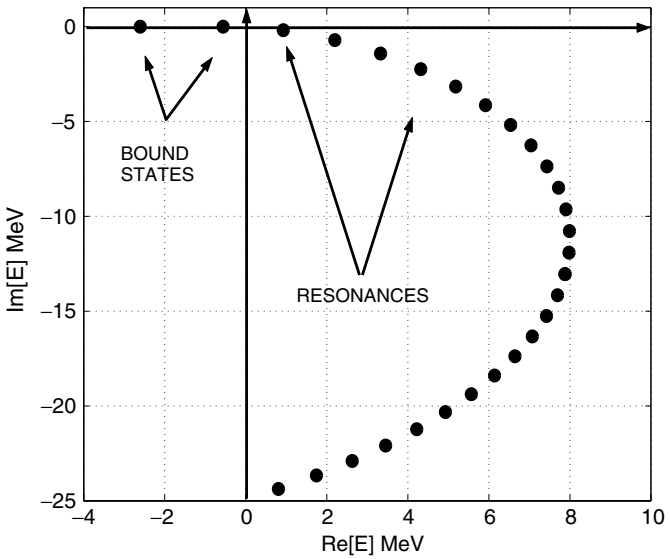

Figure 9. Plot of pole trajectory in the complex energy plane for the $l = 1$ partial wave solution of the Malfliet–Tjon interaction for v_A varied from -5.6 to -2.9 in steps of 0.1.

strength v_A is varied from -5.6 to -4.1 in steps of 0.1 MeV. For $v_A = -5.6$ and $v_A = -5.5$ we have a bound state. The calculations were performed with the contour C^+_{R+T}, rotated $\theta = \pi/4$ and translated $|\mathrm{Im}[k]| = 1.5 \sin(\pi/4)\,\mathrm{fm}^{-1} \approx 1.06\,\mathrm{fm}^{-1}$ in the fourth quadrant of the complex k-plane. Figures 10 and 11 show plots of the real and imaginary parts

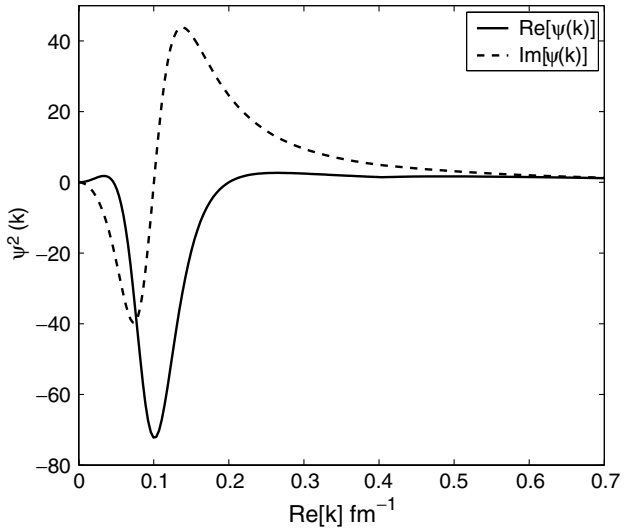

Figure 10. The square of the normalized resonance wavefunction at the resonance energy $E = 0.6554 - 0.1069\mathrm{i}$ MeV for an interaction strength $\nu_A = -5.42$ of the $l = 1$ Malfliet–Tjon interaction. In the complex k-plane this resonant pole is located at $k = 0.1261 - 0.0102\mathrm{i}\,\mathrm{fm}^{-1}$. This state is calculated using the contour C^+_{R+T} with rotation $\theta = \pi/5$ and translation $\mathrm{Im}[k] = -0.5 \times \sin(\theta)\,\mathrm{fm}^{-1}$. We have plotted the real and imaginary parts of the wavefunction as functions of real momenta along the contour C^+_{R+T}.

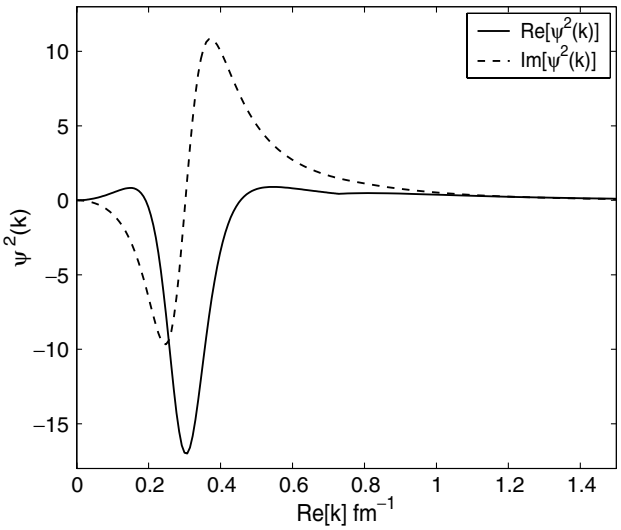

Figure 11. The squared normalized resonance wavefunction at the resonance energy $E = 5.1804 - 3.1555\mathrm{i}$ MeV for an interaction strength $\nu_A = -5$ of the Malfliet–Tjon interaction. In the complex k-plane this resonant pole is located at $k = 0.3682 - 0.1033\mathrm{i}\,\mathrm{fm}^{-1}$. This state is calculated using the contour C^+_{R+T} with rotation $\theta = \pi/5$ and translation $\mathrm{Im}[k] = -0.9 \times \sin(\theta)$. We have plotted the real and imaginary parts of the wavefunction as a function of real momenta along the rotated contour.

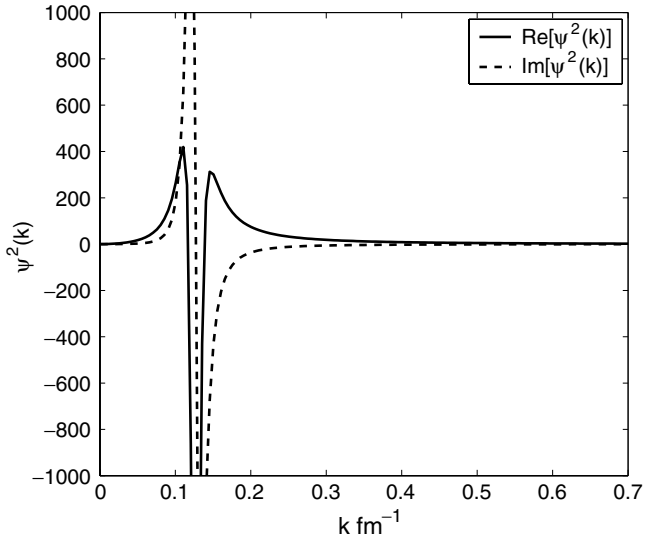

Figure 12. The square of the normalized resonance wavefunction defined along the real k-axis. The resonance energy is $E = 0.6554 - 0.1069\text{i}$ MeV for an interaction strength $v_A = -5.42$ in the $l = 1$ Malfliet–Tjon interaction. In the complex k-plane, this resonant pole is located at $k = 0.1261 - 0.0102\text{i}$ fm^{-1}.

of the squared normalized resonance wavefunction at the resonance energies $E = 0.6554 - 0.1069\text{i}$ and $5.1804 - 3.1555\text{i}$ MeV corresponding to the interaction strengths $v_A = -5.42$ and -5, respectively. The wavefunction is plotted as a function of real momenta along the contour C^+_{R+T}. In the complex k-plane, the resonance energies $E = 0.6554 - 0.1069\text{i}$ and $5.1804 - 3.1555\text{i}$ MeV corresponds to $k = 0.1261 - 0.0102\text{i}$ and $0.3682 - 0.1033\text{i}$ fm^{-1}, respectively. We see that the peak of real part of the squared resonance wavefunction is located around the real part of the resonant pole in the complex k-plane. The imaginary part of the wavefunction changes sign in the neigbourhood of the resonant pole.

The squared resonance wavefunctions plotted in figures 10 and 11 are not to be interpreted as physical momentum distributions, as they depend on the distorted contour. The physical momentum distribution of a resonant state must be defined along the real k-axis. The Berggren basis contains bound, antibound, resonant and non-resonant continuum states which are defined along the distorted contour. The transformation of these states to the real energy axis is readily done by the integral equation (2.2). All quantities on the right-hand side of equation (2.2) are known, and the integration is over the distorted contour. For k real, we get $\psi_{nl}(k)$ along the real k-axis or equivalently along the real physical energy axis. Figures 12 and 13 show plots of the squared resonance functions for $v_A = -5.42$ and -5 respectively, along the real k-axis. In figure 12, an extreme peaking of the wavefunction is observed at the real energy part of the resonant pole in the complex k-plane. This is due to the small imaginary part of the pole, and the resonance pole is located close to the real k-axis.

On the other hand, for $v_A = -5$, the behaviour of the resonance wavefunction in figure 13 is smooth and well behaved along the real k-axis. In this case, the resonance pole is rather far from the real k-axis, and no singular behaviour is observed. The calculation of resonant states along the real axis become numerically unstable for resonances with narrow widths. This is easily seen from equation (2.2), where the wavefunction becomes ill-behaved for poles close to the real axis.

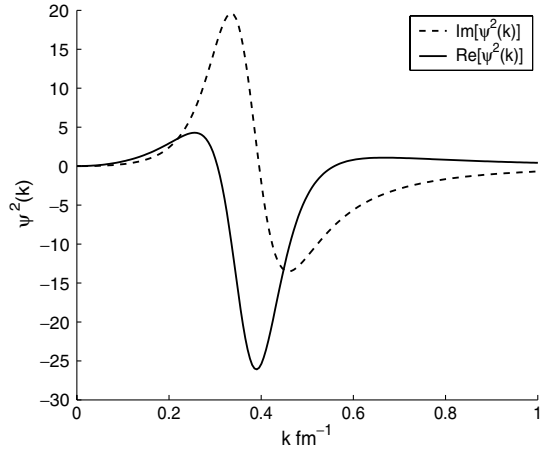

Figure 13. The squared normalized resonance wavefunction defined along the real k-axis. The resonance energy is $E = 5.1804 - 3.1555\mathrm{i}$ MeV for an interaction strength $v_A = -5$ of the Malfliet–Tjon interaction. In the complex k-plane, this resonant pole is located at $k = 0.3682 - 0.1033\mathrm{i}\ \mathrm{fm}^{-1}$.

2.4. $^1S_0$ antibound states of the CD–Bonn interaction

As an example of a currently used realistic interaction we present a calculation of the $^1\mathrm{S}_0$ antibound states in the charge-dependent Bonn interaction (CD–Bonn). The CD–Bonn interaction is given in [29]. The tensor component of the CD–Bonn interaction couples angular momentum, $l = j - 1$ and $j + 1$, in the spin triplet channel. It is straightforward to include this coupling in the formalism outlined above.

The realistic nucleon–nucleon interaction does not have a resonant structure in the low energy region $E < 300$ MeV. It does however support antibound states in the $^1\mathrm{S}_0$ isospin triplet channel and a bound state in the coupled isospin singlet channel (the deuteron) $^3\mathrm{S}_1 - {}^3\mathrm{D}_1$. We compare the calculated antibound state locations in the complex k-plane with the values obtained by the effective range approximation (see [1, 9]). In the following, we do not include Coulomb effects when considering the isospin $t_z = -1$ channel (proton–proton scattering).

The effective range approximation for the s-wave poles is given by

$$k = -\mathrm{i}\left[\sqrt{\frac{2}{r_{NN}|a_{NN}|} + \frac{1}{r_{NN}^2}} - \frac{1}{r_{NN}}\right]. \tag{2.12}$$

The theoretical (see below) and experimental values [29] for the $^1\mathrm{S}_0$ scattering lengths a_{NN} and effective range r_{NN} are given in table 2.

The antibound state poles are located on the negative imaginary k-axis. Applying CDM in this case, one has to choose a contour which extends into the third quadrant of the complex k-plane. The distorted contour C^+_{R+T} proves to be suitable contour in this case. To apply CDM by integrating along the contour C^+_{R+T} the singularities in the CD–Bonn interaction has to be determined.

The CD–Bonn interaction is given explicitly in momentum space. The derivation of the interaction is based on field theory, starting from Lagrangians describing the coupling of the various mesons of interest to nucleons [29]. The one-boson-exchange interaction is

Table 2. Scattering lengths (a) and effective ranges (r) for the $^1S_0$ channel, in units of fm. For the proton–proton channel Coulomb effects are not included.

	CD–Bonn	Experiment
a_{pp}	−17.4602	
r_{pp}	2.845	
a_{nn}	−18.9680	-18.9 ± 0.4
r_{nn}	2.819	2.75 ± 0.11
a_{np}	−23.7380	-23.740 ± 0.020
r_{np}	2.671	2.77 ± 0.05

Table 3. Calculation of antibound state energies in the $^1S_0$ isospin triplet channel by the effective range approximation (EFR) and the contour deformation method (CDM), in units of MeV. Convergence is obtained in each isospin channel. Column A used $N1 = 20$, $N2 = 30$ integration points, column B used $N1 = 20$, $N2 = 50$ integration points and column C used $N1 = 30$, $N2 = 80$ integration points. Energy E is given in units of MeV.

	CDM			EFR
	A	B	C	
T_z	E	E	E	E
−1 (pp)	−0.11766	−0.11761	−0.11761	−0.11763
1 (nn)	−0.10070	−0.10069	−0.10069	−0.10070
0 (np)	−0.06632	−0.06632	−0.06632	−0.06632

proportional to

$$V(\mathbf{k},\mathbf{q}) \propto \sum_{\alpha=\pi^0,\pi^\pm,\rho,\omega,\sigma_1,\sigma_2} \bar{V}_\alpha(\mathbf{k},\mathbf{q}) F_\alpha^2(\mathbf{k},\mathbf{q};\Delta_\alpha). \tag{2.13}$$

Both $\bar{V}_\alpha(\mathbf{k},\mathbf{q})$ and $F_\alpha^2(\mathbf{k}, q; \Delta_\alpha)$ contain terms of the form

$$\frac{1}{(\mathbf{k}-\mathbf{q})^2 + m_\alpha^2}, \tag{2.14}$$

which are of the Yukawa type. In a partial wave decomposition these Yukawa terms will be composed of Legendre functions of the second kind, $Q_l(x)$, with $x = (k^2 + q^2 + m_\alpha^2)/2kq$. The analytic structure of the CD–Bonn interaction is then seen to be that of the Malfliet–Tjon interaction, which was discussed above. The poles of the interaction are determined by the various meson masses m_α and cut-off masses Δ_α. Considering the solution of the eigenvalue problem by the contour deformation method using contour C^+_{R+T}, singularities in the interaction appear for $z = z' = \pm i m_\alpha/2$. For a rotation into the third quadrant of the complex k-plane, the maximum translation into the complex k-plane is then determined by the smallest meson mass entering the potential, which is the π-meson, $m_{\pi^0}c^2 = 134.9764$ MeV. For a given rotation into the third quadrant, i.e., $\theta \geqslant \pi/2$, we get a restriction on the translation; $\mathrm{Im}[k] < -134.9764/2/\hbar c\ \mathrm{fm}^{-1}$.

Table 3 gives results for the antibound states in the $^1S_0$ channel by the contour deformation method. A comparison with the effective range calculation of the antibound state poles is also shown. The contour was rotated by an angle $\theta = 2\pi/3$ into the complex k-plane with a subsequent translation transformation given by $\mathrm{Im}[k] = -30\ \sin(5\pi/7)/\hbar c\ \mathrm{fm}^{-1}$ (or $\mathrm{Im}[k] \approx -0.12\ \mathrm{fm}^{-1}$) in the lower-half k-plane. This is sufficient to reproduce the antibound states in the $^1S_0$ channel, as they are known to lie very close to the scattering threshold,

$k \approx -0.05\mathrm{i}\,\mathrm{fm}^{-1}$. By this contour the full energy spectrum is obtainable since it is known *a posteriori* that the $^1S_0$ channel supports only antibound states near the scattering threshold. The convergence of the numerical calculated values is demonstrated by increasing the number of integration points N.

3. Two-body scattering amplitude in a Berggren representation

3.1. Berggren expansion of the t-matrix

In effective interaction studies for finite nuclei the harmonic oscillator basis has served as a standard expansion basis for the G-matrix. This basis may work well in cases where the nucleons are well bound but less so near the nuclear driplines. The general Berggren basis has an advantage in that it is generated from the Hamiltonian of the examined problem. Expansions in this basis will increase the convergence drastically. In this section we will discuss the solution for the full off-shell t-matrix and, hence, the full two-body scattering problem, by expanding the two-body Green's function in a complete set of Berggren states. The Berggren representation of the scattering equations gives an analytic continuation in energy, from the upper rim of the cut through the cut and into the non-physical energy sheet. This has relevance for nuclear medium studies where the input energy is in general complex. In a nuclear medium calculation the self-consistently determined quasiparticle energies are in general complex.

The t-matrix is defined in operator form by

$$t(\omega) = V + Vg^{II}(\omega)V \tag{3.1}$$

or

$$t(\omega) = V + Vg_0^{II}(\omega)t(\omega). \tag{3.2}$$

Here ω is the incoming energy, $g^{II}(\omega)$ the resolvent, commonly known as the Green's operator, and $g_0^{II}(\omega)$ the corresponding free Green's operator. In operator form they are defined by

$$g_0^{II}(\omega) = \frac{1}{\omega - H_0}, \tag{3.3}$$

$$g^{II}(\omega) = \frac{1}{\omega - H}. \tag{3.4}$$

They are related through the Dyson equation

$$g^{II}(\omega) = g_0^{II}(\omega) + g_0^{II}(\omega)Vg^{II}(\omega). \tag{3.5}$$

The term H_0 is the kinetic energy operator and H the full two-body Hamiltonian. The physical interpretation of the Green's functions is that g_0^{II} describes the propagation of two noninteracting particles, whereas g^{II} describes the propagation of two interacting particles in free space.

By expanding the unit operator on a complete set of physical eigenstates of H given in equation (1.1), we can write the interacting Green's operator as

$$g^{II}(\omega) = \sum_b \frac{|\psi_b\rangle\langle\psi_b|}{\omega - E_b} + \int_0^\infty \mathrm{d}E_c \, \frac{|\psi_c\rangle\langle\psi_c|}{\omega - E_c}. \tag{3.6}$$

This is the spectral decomposition of the Greens's function. Here b denotes the discrete bound state spectrum and c the positive energy continuum. We see from this equation that the interacting Green's function is analytic in the entire complex energy plane, except

at the spectrum of the Hamiltonian including a branch cut along the positive real energy axis. In physical scattering, with outgoing waves at infinity, the energy has to approach the cut from above, i.e. $\omega \to E + \mathrm{i}\eta$. Approaching the cut from below, i.e. $\omega \to E - \mathrm{i}\eta$ corresponds to incoming waves at infinity. The discontinuity of the Green's function across the cut is

$$g^{II}(E + \mathrm{i}\eta) - g^{II}(E - \mathrm{i}\eta) = -2\pi\mathrm{i}|\psi_c\rangle\langle\psi_c|. \tag{3.7}$$

The Berggren representation of the Green's function is obtained by expanding the unit operator using the completeness relation given in equation (2.6). In this case the Green's operator takes the form

$$g^{II}(\omega) = \sum_{\alpha} \frac{|\psi_\alpha\rangle\langle\psi_\alpha^*|}{\omega - E_\alpha} + \int_{C^+} \mathrm{d}E\, \frac{|\psi\rangle\langle\psi^*|}{\omega - E}. \tag{3.8}$$

Here α denotes bound, antibound and resonant states. The integration contour C^+ denotes an arbitrary inversion symmetric contour (see e.g. figure 1), and gives the non-resonant distorted continuum contribution to the interacting Green's function. If we neglect the non-resonant continuum contribution to the Green's function we get the *resonant state expansion* of the Green's function. Such expansions have been studied over the last decade for finite range potentials (see e.g. [7, 38, 20]). The Green's function given in equation (3.8) is continuous and analytic in energy across the real axis and into the domain C of the lower part of the complex energy plane. Equation (3.8) is therefore an analytic continuation in energy of the physical Green's function given in equation (3.6).

The Berggren representation of the t-matrix is obtained by inserting the interacting Green's function given by equation (3.8) into equation (3.1), giving

$$t(\omega) = V + \Delta t(\omega) = V + \Delta t^R(\omega) + \Delta t^C(\omega). \tag{3.9}$$

Here $\Delta t^R(\omega)$ is the resonant contribution while $\Delta t^C(\omega)$ is the non-resonant distorted continuum contribution to the t-matrix. By projecting $t(\omega)$ on momentum states, and decomposing into partial waves, the t-matrix elements $t_l(k, k'; \omega)$ can be expressed as one-dimensional integral equations,

$$t_l(k, k', \omega) = V_l(k, k') + \frac{4}{\pi^2} \int_{C^+} \int_{C^+} \mathrm{d}q\, \mathrm{d}q'\, q^2 q'^2 V_l(k, q) g^{II}(q, q'; \omega) V_l(q', k'). \tag{3.10}$$

This representation of the t-matrix is valid as long as we do not pass through any singularities of the interaction potential by deforming the real k-axis into the distorted contour C^+. The interacting Green's function on the inversion symmetric contour C^+ is given by

$$g^{II}(k, k'; \omega) = \sum_{\alpha} \frac{\psi_\alpha(k)\psi_\alpha(k')}{\omega - E_\alpha} + \int_{C^+} \mathrm{d}E\, \frac{\psi_E(k)\psi_E(k')}{\omega - E}. \tag{3.11}$$

Equation (3.10) has the same analytic structure as the Green's function of equation (3.8), except for possible singularities in the interaction potential. Using equation (2.2), the on-shell t-matrix may be written as

$$t_l(k, k, \omega = \hbar^2 k^2/2m_{np}) = V_l(k, k) + \sum_{\alpha} (\omega - E_\alpha)\psi_\alpha^2(k) + \int_{C^+} \mathrm{d}E\, (\omega - E)\psi_E^2(k). \tag{3.12}$$

The s-matrix is given in terms of the on-shell t-matrix by

$$s_l(k) = 1 - 2\frac{m_{np}}{\hbar^2} \mathrm{i}k\, t_l(k, k, \omega). \tag{3.13}$$

Here the resonant and non-resonant wavefunctions defined along the real k-axis enters the equations. The absolute value of the s-matrix is then a valuable test on how accurate our numerical calculations are. Applying CDM enables us to obtain $t_l(k, k'; \omega)$ for both real and complex energies ω. The integral becomes non-singular on the deformed contour for real and positive input energies ω, resulting in numerically stable solutions for physical two-body scattering.

The Berggren representation of the t-matrix also allows for a separate study of the resonant and continuum contributions. The limitation of this method is due to the fact that most potentials in momentum space have singularities in the complex plane when one argument is real and the other is complex. By applying contour C_R^+, which is based on rotation into the complex plane, in most cases there will be restrictions on both rotation angle (θ) and maximum incoming and outgoing momentum (k, k') (see e.g. [16]). Using a contour of the type C_{R+T}^+, we can avoid these limitations by choosing the integration contour in such a way that the potential singularities always will lie outside the integration contour and, therefore, do not give any restriction on rotation angle and maximum incoming and outgoing momentum. By an appropriate choice of contour, CDM gives an alternative to the standard principal value prescription in solving for the t-matrix. In addition, it allows for a separate study of the resonant contribution to the full scattering amplitude. In the case of narrow resonances, the resonant contribution to the t-matrix will dominate strongly over the continuum contribution around the resonance energy. This separation is motivated by the fact that the most interesting phenemenon taking place in the continuum is the resonance phenomenon.

3.2. t-matrix for the Malfliet–Tjon interaction using a Berggren basis

In addition to giving accurate calculation of the complete energy spectrum on the second sheet, CDM provides also a basis for a calculation of the fully off-shell two-body scattering amplitude (t-matrix). Here we present calculations of the t-matrix and phase shifts for the Malfliet–Tjon interaction using the C_{R+T}^+ contour. The phase shifts are given in terms of the t-matrix elements by

$$\delta_l(k) = \arctan \frac{\mathrm{Im}[t_l(k, k; \omega)]}{\mathrm{Re}[t_l(k, k; \omega)]}, \tag{3.14}$$

where the input energy ω is given on-shell, i.e. $\omega = \hbar^2 k^2/2m_{np}$. If the t-matrix is approximated by the resonant part $t \approx \Delta t^R$, one gets the famous Breit–Wigner approximation to the phase shifts (see e.g. [9])

$$\delta_l(k) \approx \delta^R(k) = \arctan\left(\frac{\Gamma/2}{E - E_R}\right) + \delta^b \tag{3.15}$$

valid for narrow widths Γ and in a small energy range around the resonance energy. The motivation for using the contour C_{R+T}^+ in calculation of the t-matrix is based on the analytic properties of the interaction. For real incoming and outgoing momenta we have to face the problem of avoiding the singularity in the interaction $V(k, k')$, located at $\mathrm{Im}[k] = \pm\mu/2$. By using the contour C_{R+T}^+ this problem is solved, and stable solution of the t-matrix can be obtained. Using the spectral decomposition of the Green's function, a separate analysis

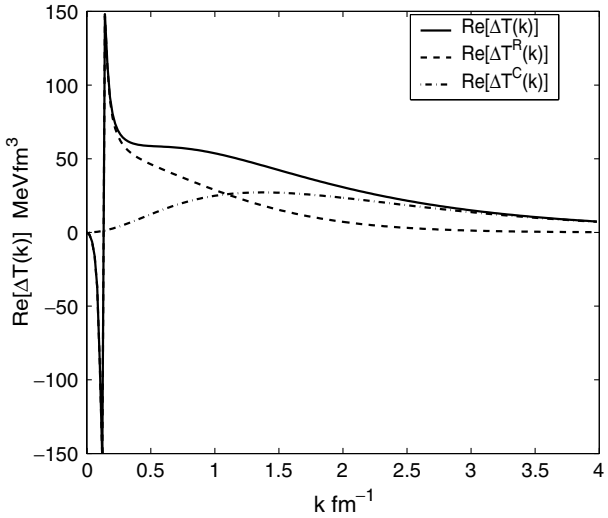

Figure 14. Real part of continuum $\Delta T^C(k)$ and resonant $\Delta T^R(k)$ contributions to the on-shell t-matrix, for the Malfliet–Tjon interaction with strength $v_A = -5.42$ supporting a resonance at energy $E = 0.6554 - 0.1069\mathrm{i}$ MeV.

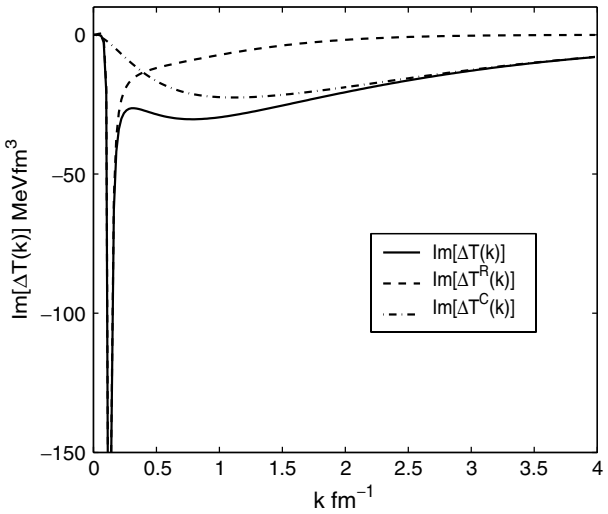

Figure 15. Imaginary part of continuum $\Delta T^C(k)$ and resonant $\Delta T^R(k)$ contributions to the on-shell t-matrix, for the Malfliet–Tjon interaction with strength $v_A = -5.42$ supporting a resonance at energy $E = 0.6554 - 0.1069\mathrm{i}$ MeV.

of the resonant and continuum contributions can be performed. We will see below that in the case of a short-range interaction of the Yukawa type, the continuum contribution is non-neglible in most of phase-space, except in a small phase volume around the resonance energy.

Figures 14 and 15 give plots of the real and imaginary parts of Δt, Δt^C and Δt^R. The t-matrix elements were evaluated on-shell. The calculations were done for $v_A = -5.42$ and $l = 1$ Malfliet–Tjon interaction, giving a resonance pole at $k = 0.13 - 1.02\mathrm{i}\,\mathrm{fm}^{-1}$ in

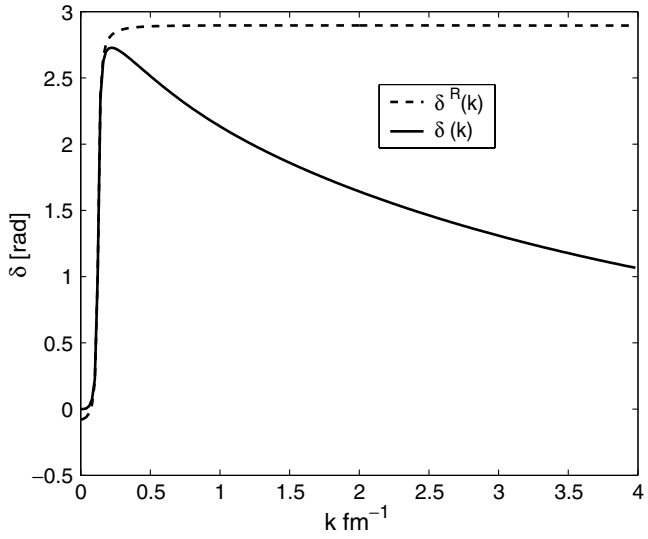

Figure 16. Plot of phase shift for the Malfliet–Tjon interaction with strength $v_A = -5.42$ supporting a resonance at energy $E = 0.6554 - 0.1069\mathrm{i}$ MeV. The broken line gives the resonant contribution to the phase shift.

Table 4. Numerical calculations of the absolute value of the s-matrix for various on-shell momenta. The calculations were done with the $l = 1$ Malfliet–Tjon interaction given on the distorted contour C^{+}_{R+T} rotated $\theta = \pi/5$ and translated $\mathrm{Im}[k] = -1.5\sin(\pi/5)\ \mathrm{fm}^{-1} \approx -0.8817\ \mathrm{fm}^{-1}$ into the fourth quadrant of the complex k-plane.

k (fm^{-1})	$\lvert s_l(k)\rvert$
0.1	0.9999985
1	0.9999999
2	0.9999998
3	0.9999996
4	1.0000017

the complex k-plane. The calculations used a rotation angle $\theta = \pi/5$ and a translation $|\mathrm{Im}[k]| = 1.5\sin(\pi/5) \approx 0.8817\,\mathrm{fm}^{-1}$, and 50 integrations points along the line segments $\mathbf{L}_1$ and $\mathbf{L}_2$, respectively. The resonance energy is located rather close to the real energy axis, and that the resonance part of the t-matrix dominates strongly over the continuum part around the real part of the pole $\mathrm{Re}[k] = 0.13\,\mathrm{fm}^{-1}$. This behaviour justifies the Breit–Wigner approximation to the phase shifts in this energy region.

Figure 16 shows the complete phase shifts, δ, including both non-resonant continuum and resonant contributions, and the resonant contribution, δ^R. In the vicinity of the resonance energy, δ^R gives a good approximation to the full phase shift. Table 4 gives the absolute value of the s-matrix (see equation (3.13)) for various on-shell momenta, and we see that the numerical accuracy is rather good. The accuracy increases with number of integration points used in the calculations.

By decreasing the interaction strength v_A the resonant poles moves further down into the lower-half k-plane. The contribution to the phase shifts and the t-matrix elements from resonances far from the real energy axis is expected to be small. Figure 17 shows the complete

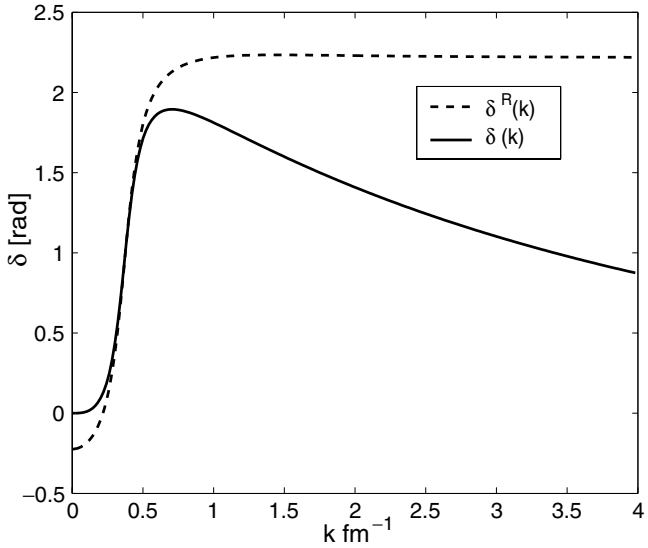

Figure 17. Plot of phase shift for the Malfliet–Tjon interaction with strength $v_A = -5$, supporting a resonance at energy $E = 5.1804 - 3.1555\mathrm{i}$ MeV. The broken line gives the resonant contribution to the phase shift.

and the resonant part of phase shifts for the $v_A = 5$ Malfliet–Tjon interaction, for a 'deep-lying' resonance.

4. An analytically solvable non-local two-body potential

4.1. Energy spectrum and t-matrix for the Yamaguchi interaction

It is instructive to check the CDM for an analytically solvable case, that of the non-local separable potential given by Yamaguchi [31]; it models s- and p-waves. The coordinate representation of the Yamaguchi interaction is given by a product of two Yukawa terms (see e.g. [10]). A separable interaction in coordinate space gives a separable interaction in momentum space, and is analytically solvable (see e.g. [1] for a demonstration). The Yamaguchi interaction therefore admits analytic solution of the full off-shell t-matrix and the t-matrix poles, corresponding to the energy spectrum. The Yamaguchi s-wave potential supports bound and antibound states, while the Yamaguchi p-wave potential supports bound, antibound and resonant states. The Yamaguchi potential is therefore useful in modelling loosely bound two-body systems which may have a rich resonant state structure, and for checking the numerics in calculations of the t-matrix and the energy spectrum.

The s-wave Yamaguchi potential has the form

$$V_0(k,q) = -\lambda g_0(k) g_0(q), \tag{4.1}$$

where

$$g_0(k) = \frac{1}{k^2 + \beta^2}. \tag{4.2}$$

The full off-shell t-matrix for the s-wave potential reads [1]

$$t_0(k,q;\omega) = -\lambda \frac{g_0(k) g_0(q)}{1 - \Delta_0(\omega)}, \tag{4.3}$$

where we have defined

$$\Delta_0(\omega) \equiv \lambda \frac{2}{\pi} \int_0^\infty \mathrm{d}k \, \frac{k^2 (g_0(k))^2}{\hbar^2 k^2/2m - \omega}. \tag{4.4}$$

The integral $\Delta_0(\omega)$ can be evaluated analytically. For $\omega = \hbar^2 k_0^2/2m$ we get

$$\Delta_0(k_0) = \lambda \frac{m}{\hbar^2} \frac{(\beta + \mathrm{i}k_0)^2}{\beta(\beta^2 + k_0^2)^2}. \tag{4.5}$$

For bound and antibound states the t-matrix poles are located along the positive and negative imaginary k-axis, respectively. Writing $\kappa = -\mathrm{i}k_0$, where κ is a real quantity, we can solve for the t-matrix poles as zeros of the denominator, $1 - \Delta_0(k_0) = 0$, giving in terms of κ,

$$\kappa = -\beta \pm \sqrt{\frac{\lambda m}{\beta \hbar^2}}, \tag{4.6}$$

and we see that the poles are located along the imaginary k-axis. For $\lambda > \beta^3 \hbar^2/m$, we get a bound ($\kappa > 0$) and an antibound state ($\kappa \leqslant 0$), and for $\lambda \leqslant \beta^3 \hbar^2/m$, we get two antibound states.

The separable p-wave interaction is given by

$$V_1(k, q) = -\lambda g_1(k) g_1(q), \tag{4.7}$$

where

$$g_1(k) = \frac{k}{k^2 + \beta^2}, \tag{4.8}$$

and the t-matrix becomes [1]

$$t_1(k, q; E) = -\lambda \frac{g_1(k) g_1(q)}{1 - \Delta_1(k_0)}. \tag{4.9}$$

Here

$$\Delta_1(\omega) \equiv \lambda \frac{2}{\pi} \int_0^\infty \mathrm{d}k \, \frac{k^2 (g_1(k))^2}{\hbar^2 k^2/2m - \omega}. \tag{4.10}$$

The integral $\Delta_1(E)$ can be calculated analytically, giving in terms of k_0,

$$\Delta_1(k_0) = \lambda \frac{m}{\hbar^2} \frac{\beta^3 + k_0^2(3\beta + 2\mathrm{i}k_0)}{(\beta^2 + k_0^2)^2} \tag{4.11}$$

solving for the poles gives in terms of $\kappa = -\mathrm{i}k_0$,

$$\kappa = \lambda \frac{m}{\hbar^2} - \beta \pm \sqrt{\lambda \frac{m}{\hbar^2} \left(\lambda \frac{m}{\hbar^2} - \beta \right)}. \tag{4.12}$$

We see that for p-waves the interaction supports bound, antibound and resonant states. The bound state condition is

$$\lambda > \frac{\beta \hbar^2}{m} \tag{4.13}$$

giving in addition an antibound state. The interaction has a branchpoint at $k = 0$, where the bound and antibound states meet and move symmetrically from the imaginary axis into the lower-half k-plane giving capture and decay resonant states. Figure 18 shows the pole trajectory for the Yamaguchi p-wave interaction.

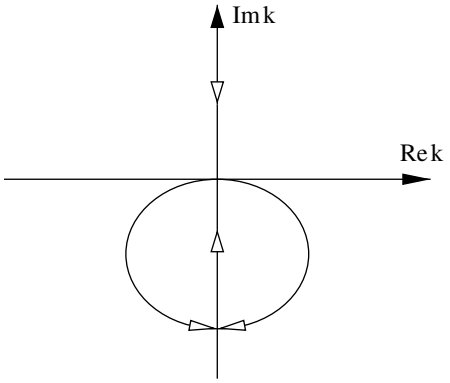

Figure 18. Pole trajectory for the p-wave Yamaguchi interaction in the complex k-plane.

4.2. Expansion of the Yamaguchi eigenvalue problem on a Berggren basis generated from the Malfliet–Tjon interaction

Here we illustrate the flexibility of the Berggren basis as an expansion basis for a more general interaction. The Yamaguchi eigenvalue problem will be expanded on a Berggren basis, again generated from the Malfliet–Tjon interaction. It is interesting to observe the convergence of eigenvalues as the number of non-resonant continuum states increases. Does the fact that the Yamaguchi interaction is non-local whereas the Malfliet–Tjon interaction giving rise to the basis is local, influence the applicability of the Berggren basis, and the convergence of the eigenvalue problem? A numerical investigation of this is carried out below. The numerically determined eigenvalues as a function of basis elements will be compared with the analytical solutions of the eigenvalues.

The Hamiltonian eigenvalue problem expanded on a general Berggren basis takes the abstract form

$$\sum_{\gamma}\langle\varphi_{\alpha}^{*}|T+V|\varphi_{\gamma}\rangle c_{\gamma}=E\sum_{\gamma}\delta_{\gamma,\alpha}c_{\gamma}, \tag{4.14}$$

where the expansion coefficients c_γ fulfil the completeness relation $\sum_\gamma c_\gamma^2 = 1$. In momentum space, the matrix elements of the kinetic and potential operators take the form

$$\langle\varphi_{\alpha}^{*}|T|\varphi_{\gamma}\rangle=\frac{2}{\pi}\int_{C^{+}}\mathrm{d}k\,k^{2}\varphi_{\alpha,l}(k)\frac{\hbar^{2}}{2m}k^{2}\varphi_{\gamma,l}(k) \tag{4.15}$$

$$\langle\varphi_{\alpha}^{*}|V|\varphi_{\gamma}\rangle=\frac{4}{\pi^{2}}\int_{C^{+}}\mathrm{d}k\,k^{2}\int_{C^{+}}\mathrm{d}k'\,k'^{2}\varphi_{\alpha,l}(k)V_{l}(k,k')\varphi_{\gamma,l}(k'). \tag{4.16}$$

We consider solutions for the $l = 1$ Yamaguchi interaction with $\beta = 2\,\mathrm{fm}^{-1}$ and varying interaction strength λ. This interaction supports bound states for $\lambda > 2\hbar^2/m \approx 165.883\,\mathrm{MeV\,fm}^{-1}$. Table 5 gives numerical results for bound and resonant states of the $l = 1$ Yamaguchi interaction. The Berggren basis was generated by the $l = 1$ Malfliet–Tjon interaction given on the distorted contour C^{+}_{R+T} rotated $\theta = \pi/5$ and translated $\mathrm{Im}[k] = -\sin(\pi/5)\ \mathrm{fm}^{-1} \approx -0.59\ \mathrm{fm}^{-1}$ into the fourth quadrant of the complex k-plane. The calculations used 50 integration points along the rotated and translated parts of the contour.

Table 5. Numerical calculations of bound and resonant states of the $l = 1$ Yamaguchi interaction of strength λ. The Berggren basis was generated by the $l = 1$ Malfliet–Tjon interaction given on the distorted contour C^{+}_{R+T} rotated $\theta = \pi/5$ and translated $\mathrm{Im}[k] = -\sin(\pi/5)\ \mathrm{fm}^{-1} \approx -0.59\,\mathrm{fm}^{-1}$ into the fourth quadrant of the complex k-plane. Comparison is done with exact energy values for the bound and resonant states. λ is given in units of MeV fm and energy in units of MeV.

	CDM		Exact	
λ	Re[E]	Im[E]	Re[E]	Im[E]
169	−4.09667119	0	−4.09667119	0
166	−0.12337977	0	−0.12337977	0
165	0.87360132	−0.12850277	0.87360132	−0.12850277
164	1.84025247	−0.39895705	1.84025247	−0.39895705
163	2.78279024	−0.75351046	2.78279024	−0.75351046
160	5.46572327	−2.17613872	5.46572327	−2.17613872

Table 6. Numerical calculations of antibound states in the $l = 1$ Yamaguchi interaction. The Berggren basis was generated by the $l = 1$ Malfliet–Tjon interaction given on the distorted contour C^{+}_{R+T} rotated $\theta = 2\pi/3$ and translated $\mathrm{Im}[k] = -\sin(2\pi/3)\,\mathrm{fm}^{-1} \approx -0.87\,\mathrm{fm}^{-1}$ into the third quadrant of the complex k-plane. Comparison is done with exact energy values for the antibound states. Calculations used 50 integration points along the rotated and translated lines. λ is given in units of MeV fm and energy in units of MeV.

	CDM		Exact	
λ	Re[E]	Im[E]	Re[E]	Im[E]
168	−1.689679639	0	−1.689679639	0
167	−0.948105835	0	−0.948105835	0
166	−0.110946667	0	−0.110946633	0

The singularity structure of the Yamaguchi interaction is particularly simple, having poles only for $\mathrm{Im}[k] = \pm\beta$. Therefore, any contour in the fourth quadrant will do. The interaction parameters for the Malfliet–Tjon interaction, used for the Berggren basis, are the same as in previous sections with $\nu_A = -5$ supporting a resonance at $E = 5.1804 - 3.1555\mathrm{i}$ MeV.

Table 6 gives numerical results for antibound states in the $l = 1$ Yamaguchi interaction. The Berggren basis was generated by the $l = 1$ Malfliet–Tjon interaction given on the distorted contour C^{+}_{R+T} rotated $\theta = 2\pi/3$ and translated $\mathrm{Im}[k] = \sin(\pi/5)\,\mathrm{fm}^{-1} \approx 0.87\,\mathrm{fm}^{-1}$ into the third quadrant of the complex k-plane. The calculations again used 50 integration points and the same input as above. The agreement with exact results is convincing for all three cases: bound, resonant and antibound.

5. Expansion of resonances of a Gaussian potential on a Berggren basis generated by the Malfliet–Tjon interaction

We finally consider the frequently used local Gaussian potential

$$V(r) = V_0 \exp(-r^2\alpha^2), \tag{5.1}$$

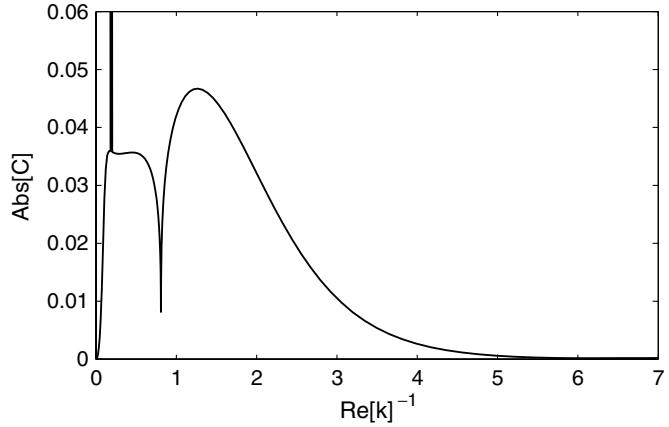

Figure 19. Plot of the absolute value of the coefficients of the Malfliet–Tjon Berggren expansion of a resonant state generated by a Gaussian potential. The coefficients are plotted as a function of $\mathrm{Re}[k]\ \mathrm{fm}^{-1}$.

which in momentum space takes the analytic form

$$V_l(k,k') = V_0 \frac{\pi}{4\alpha^2} \frac{1}{\sqrt{kk'}} \exp\left(-\left(\frac{k^2+k'^2}{4\alpha^2}\right)\right) I_{l+1/2}\left(\frac{kk'}{2\alpha^2}\right). \tag{5.2}$$

Here $I_{l+1/2}(z)$ is a Bessel function of the first kind with complex arguments. In the complex k-plane, the Gaussian potential diverges exponentially for $|\mathrm{Im}[k]| > |\mathrm{Re}[k]|$. Solving the momentum space Schrödinger equation on a rotated contour C_R^+, we get the restriction $\theta < \pi/4$ on the rotation angle. On the other hand, we may choose a contour of the type C_{R+T}^+ and this problem is resolved, allowing for an continuation in the third quadrant of the complex k-plane.

For a range $\alpha = 1.8\,\mathrm{fm}^{-2}$ and a depth $V_0 = 150\,\mathrm{MeV}$ for the $l = 1$ Gaussian potential, the CDM gives a resonance with energy $E = 0.676131964 - 0.157257363\mathrm{i}\,\mathrm{MeV}$. This resonance was calculated on the C_{R+T}^+ contour, rotated $\theta = \pi/5$ and translated $\mathrm{Im}[k] = -\sin(\pi/5)\,\mathrm{fm}^{-1} \approx 0.5878\,\mathrm{fm}^{-1}$. The Berggren basis was generated from the $l = 1$ Malfliet–Tjon interaction with $\nu_A = -5.42$ supporting a resonance with energy $E = 0.655473351 - 0.106928706\mathrm{i}\,\mathrm{MeV}$.

Figure 19 gives the expansion coefficients of the Berggren basis as a function of the real part of the momentum. The spike at $\mathrm{Re}[k] \approx 0.1\,\mathrm{fm}^{-1}$ is due to the large overlap between the resonant wavefunctions of the Malfliet–Tjon and the Gaussian interaction, respectively. The discontinuity around $\mathrm{Re}[k] \approx 0.7\,\mathrm{fm}^{-1}$ has no physical meaning, and is due to the discontinuity in the deformed contour, where the rotated part goes into the translated part. From the distribution of the expansion coefficients one sees that the major contribution from the complex continuum occurs for $\mathrm{Re}[k] < 5\,\mathrm{fm}^{-1}$. On the basis of this observation, one would expect that a cutoff for a given momentum $\mathrm{Re}[k] > 5\,\mathrm{fm}^{-1}$ in the Berggren basis, would not influence the calculation of the resonant state and energy. Table 7 shows the convergence of the resonant energy as a function of cutoff in the Berggren basis. For $\mathrm{Re}[k] > 5\,\mathrm{fm}^{-1}$ the energy has converged satisfactorily.

Figures 20 and 21 show how the corresponding resonant wavefunction converges to the 'exact' wavefunction, and the sensitivity of the resonance wavefunction to cutoff in momentum. We observe that for a cutoff in momentum less than $5\,\mathrm{fm}^{-1}$, the tail of the wavefunction is not that well reproduced, even though the resonant energy has converged

Table 7. Resonant energy of the Gaussian potential discussed above as a function of cutoff in momentum/energy in the Berggren basis generated by the Malfliet–Tjon potential. The cutoff momentum is given in units of fm^{-1} and energy in units of MeV.

Cutoff	Re[E]	Im[E]
1	5.32123	0.53077
3	0.74272	−0.02750
5	0.67748	−0.15758
10	0.67698	−0.15742
20	0.67619	−0.15727
30	0.67614	−0.15726
40	0.67613	−0.15725
Exact	0.67613	−0.15725

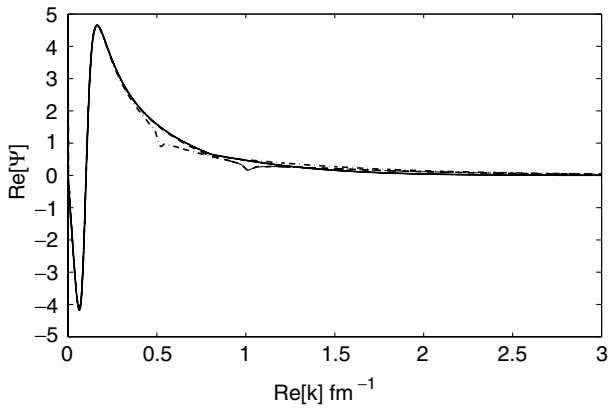

Figure 20. Plot of the real part of the resonant wavefunction generated by the Gaussian potential discussed above. The continuous line is the exact wavefunction, the broken line is the Berggren expanded wavefunction with a cutoff in momentum, $\mathrm{Re}[k] = 1\ \mathrm{fm}^{-1}$ and the dashed-dotted line with a cutoff $\mathrm{Re}[k] = 0.5\ \mathrm{fm}^{-1}$.

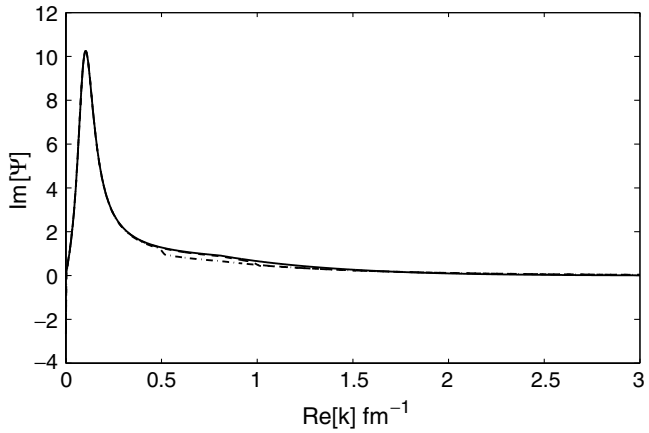

Figure 21. Plot of the imaginary part of the resonant wavefunction generated by the Gaussian potential discussed above. The continuous line is the exact wavefunction, the broken line is the Berggren expanded wavefunction with a cutoff in momentum, $\mathrm{Re}[k] = 1\ \mathrm{fm}^{-1}$ and the dashed-dotted line with a cutoff $\mathrm{Re}[k] = 0.5\ \mathrm{fm}^{-1}$.

satisfactorily for a cutoff $\mathrm{Re}[k] = 5\,\mathrm{fm}^{-1}$. The interior part of the momentum space resonant wavefunction is, on the other hand, well reproduced in both cases considered. Translated into the coordinate space picture, this reflects that in the cases of loosely bound or resonant states the correct tail of the wavefunction is important for reproducing the correct energy.

6. Conclusions and perspectives

A generalized CDM in momentum space has been presented. The deformation of the integration contour is generalized to rotation followed by translation in the complex k-plane. This generalization makes it possible to handle both *dilation* and *non-dilation* invariant potentials. We have, via chosen examples from subatomic physics, shown this to be a powerful procedure for studying resonances and antibound states in two-body systems. The method has also been successfully applied to the calculation of the full off-shell t-matrix.

The CDM allows for stable numerical calculations of binary bound states, resonances and antibound states, in addition to yielding a fully complex on- and off-shell scattering matrix, starting with a realistic nucleon–nucleon interaction. This also allows for several interesting applications and extensions of shell model type formulations. One of the major challenges in the microscopic description of weakly bound dripline nuclei is a proper treatment of both the many-body correlations and the continuum of positive energies and decay channels. Such nuclei pose a tough challenge for traditional nuclear structure methods, based essentially on the derivation of effective interactions and the nuclear shell-model (see e.g. [40] for a review). In the traditional approaches only bound states typically enter the determination of an effective interaction, be it either based upon various many-body schemes or more phenomenologically inspired approaches. Coupled with large-scale shell model studies, several properties of stable nuclei are well reproduced. However, weakly bound nuclei have a strong coupling to unbound states, either resonances or antibound states, as described in, for example, [4–6]. This implies in turn that an effective interaction should reflect such couplings with the continuum, i.e. a consistent many-body scheme should include bound states, resonances and antibound states as well.

The aim of this work has been to establish the formalism for the free scattering case, basing the analysis on schematic and realistic nucleon–nucleon interactions. Work on extension to Borromean halo systems [39] in few-body cluster models with more than two constituents, is in progress.

In forthcoming papers, we will discuss the application of binary CDM to shell model type formulations for dripline nuclei, extensions to few-body halo models and also complex interactions of particular relevance for nuclear reactions.

Acknowledgments

This work has been supported by the Research Council of Norway. We thank Boris V Danilin and Maxime Kartamyshev for stimulating discussions.

References

[1] Newton R G 1982 *Scattering Theory of Waves and Particles* (New York: Springer)
[2] Liotta R J, Maglione E, Sandulescu N and Vertse T 1996 *Phys. Lett.* B **367** 1
[3] Id Betan R, Liotta R J, Sandulescu N and Vertse T 2003 *Phys. Rev.* C **67** 014322
[4] Michel N, Nazarewicz W, Płoszajczak M and Bennaceur K 2002 *Phys. Rev. Lett.* **89** 042502
[5] Michel N, Nazarewicz W, Płoszajczak M and Okołowicz J 2003 *Phys. Rev.* C **67** 054311

[6] Id Betan R, Liotta R J, Sandulescu N and Vertse T 2002 *Phys. Rev. Lett.* **89** 042501
[7] Vertse T, Curutchet P, Liotta R J and Bang J 1989 *Acta Phys. Hungaria* **65** 305
[8] Id Betan R, Liotta R J, Sandulescu N and Vertse T 2004 *Phys. Lett.* B **584** 48
[9] Kukulin V I, Krasnopol'sky V M and Horáček J 1989 *Theory of Resonances* (Amsterdam: Kluwer Academic)
[10] Sitenko A G 1971 *Lectures in Scattering Theory* (Oxford: Pergamon)
[11] Baz' A I, Zel'dovich Ya B and Perelomov A M 1966 *Scattering, Reactions and Decay in Nonrelativistic Quantum Mechanics* (Moscow: Fiziko-Matematicheskoi Literatury)
[12] Afnan I R 1991 *Aust. J. Phys.* **44** 201
[13] Aguilar J and Combes J M 1971 *Commun. Math. Phys.* **22** 269
[14] Balslev E and Combes J M 1971 *Commun. Math. Phys.* **22** 280
[15] Brayshaw D 1968 *Phys. Rev.* **176** 1855
[16] Nuttall J and Cohen H L 1969 *Phys. Rev.* **188** 1542
[17] Stelbovics A T 1978 *Nucl. Phys.* A **288** 461
[18] Glöckle W 1978 *Phys. Rev.* C **18** 18
[19] Berggren T 1968 *Nucl. Phys.* A **109** 265
[20] Lind P 1993 *Phys. Rev.* C **47** 1903
[21] Moiseyev N 1998 *Phys. Rep.* **302** 211
[22] Csoto A 1994 *Phys. Rev.* C **49** 2244
[23] Garrido E, Fedorov D V and Jensen A S 2002 *Nucl. Phys.* A **708** 277
[24] Raskinyte I 2002 Resonances in few-body systems *PhD Thesis* University of Bergen, unpublished
[25] Nuttall J 1967 *J. Math. Phys.* **8** 873
[26] Tiktopoulos G 1964 *Phys. Rev.* **136** 275
[27] Aoyama S 2002 *Phys. Rev. Lett.* **89** 052501
[28] Pearce B C and Afnan I R 1984 *Phys. Rev.* C **30** 2022
[29] Machleidt R 2001 *Phys. Rev.* C **63** 024001
[30] Malfliet R A and Tjon J A 1969 *Nucl. Phys.* A **127** 161
[31] Yamaguchi K 1954 *Phys. Rev.* **95** 1628
[32] Gyarmati B and Vertse T 1971 *Nucl. Phys.* A **160** 523
[33] Berggren T 1971 *Nucl. Phys.* A **169** 353
[34] Berggren T 1978 *Phys. Lett.* B **73** 389
[35] Berggren T 1996 *Phys. Lett.* B **373** 1
[36] Brown L, Fivel D, Lee B W and Sawyer R 1963 *Ann. Phys.* **23** 167
[37] Elster Ch, Thomas J H and Glöckle W 1998 *Few-Body Systems* **24** 55
[38] Vertse T, Liotta R J and Maglione E 1995 *Nucl. Phys.* A **584** 13
[39] Zhukov M V, Danilin B V, Fedorov D V, Bang J M, Thompson I J and Vaagen J S 1993 *Phys. Rep.* **231** 151
[40] Hjorth-Jensen M, Kuo T T S and Osnes E 1995 *Phys. Rep.* **261** 125